International Information and Engineering Technology Association
Advancing the World of Information and Engineering

Glycerol /Phthalic Anhydride Novel Nano Composite for Microwave Absorbing Applications

Batool Abdul Rasool Zaki[1*], Farhan Lafta Rashid[2], Mohammad N. Al-Baiati[1]

[1] Department of Chemistry, College of Education for Pure Sciences, University of Kerbala, Karbala 56001, Iraq
[2] Department of Petroleum Engineering, College of Engineering, University of Kerbala, Karbala 56001, Iraq

Corresponding Author Email: Batool.abdulrasool@s.uokerbala.edu.iq

ABSTRACT

High-efficiency radar wave absorbing material was prepared utilizing nanoparticles poly (glycerol /phthalic anhydride), and the effect of using these nanocomposites with thermal paint on the properties of electromagnetic absorbing was analyzed and investigated. Results show that when the percentage of nano polymers is increased from 1% to 3%, with the presence of 2.5% of iron oxide, the reflectivity loss value rises dramatically. For the reflectivity up to 27.2dB at a frequency of 8.3 GH and a bandwidth of (8.1-8.2GH), there is a clear attenuation of the radar waves, which is confined within a bandwidth of GH (9-9.3GH). This material can be utilized as a high- efficiency radar wave absorbing applications.

1. INTRODUCTION

Research into radar absorption materials (RAMs) has been a hot topic among scientists since the development of military radar systems that can identify defence-based devices. With the fast growth of wireless technologies, digital gadgets, and radar systems, electromagnetic (EM) waves have become significant pollution sources that are hazardous to human physical health and national defense security. Microwave absorbing materials (MAMs) are used to attenuate undesired electromagnetic radiation in order to reduce the danger. Because of its high-resolution imagery and improved target recognition, radar systems of X-band frequency are widely recognized in the military industry [1]. Due to its spectacular and prospective uses in the realm of current stealth technology, radar-absorbent materials (RAMs) have garnered a lot of interest from researchers since the end of World War II [2]. Thin absorbing materials, low weight, have a broad absorption band, and have high absorption efficiency are excellent and may be considered to be an ideal material [3]. The absorbing material must also have oxidation resistance, high-temperature resistance, strong mechanical qualities, and so on, to suit the demands of certain applications. New multi-functional wave absorbing materials and high-performance wave absorbers are being developed across the world as radar wave detecting technology continues to advance [4]. Microwave absorbers have been the subject of a lot of study in the last decade. carbon fibers, carbon coils, porous carbon, graphite, and other dielectric loss materials were the subject of early study [5-10]. According to a survey of the literature, despite the numerous research on microwave absorbing materials, no prior results on the problem of improving the microwave absorbing techniques are accessible to the authors' knowledge. As a result, the goal of this research is to prepare and characterize the ability of the prepared nanocomposite materials to absorb the microwave. The influence of several relevant factors like nanopolymer weight mixing and nano Fe_3O_4 weight mixing will be investigated.

A material's shielding efficiency (SET) may be defined as the percentage of electromagnetic energy it blocks as it travels through it [11-13]. As seen in Figure 1, electromagnetic waves may interact with a variety of different materials. When electromagnetic waves land on the front face of the material, some of the force (PI) (PR) is reflected, while some of the force (PI) (PR) as energy is absorbed and dissipated, and the remaining force (PT) is transferred via the material of shielding. This means that the total attenuation is a result of a combination of three separate processes, namely, multiple internal interactions (SEM), absorption (SEA), and reversion (SER) [11, 14-17].
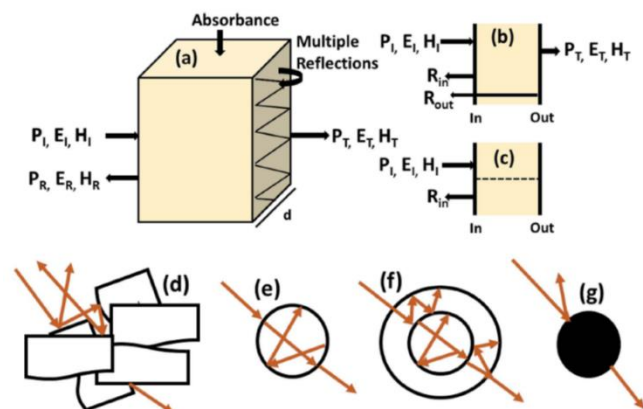
(a) Schematic diagram of electro-magnetic field intensities, transmitted power, reflected, and an incident. (b) and (c) thin sample reflection resources. (d–g) in the instance of a solid spherical, a structural multiple shells, a hollow structure, and a porous structure [18].

Figure 1. Electromagnetic waves interacting with a variety of different materials

$$SET = 10log\frac{p1}{p1} - 20log\frac{E1}{ET} - 20log\frac{HI}{HT} = SER + SEA + SEM \quad (1)$$

where, T is the transmitted, R is the reflected, and I is the incident components, while H, E, and P denote the magnetic field, electric, and energy intensities respectively [19]. Thus, SER stands for net interaction and represents the protection of SEA due to uptake. Note that the SEM can be neglected due to the contributions from secondary interactions (the output interface), then the formula could be written as [20-23]:

$$SET = SER + SEA \quad (2)$$

The basic mechanism of an electromagnetic interference shield (SER) is interaction. The echo loss (SER) refers to the mismatch of relative impedance between the EM waves and the shielding material surface. The value of the reaction loss can be determined by [24]:

$$SER = 20log\frac{z°}{4zin} = 39.5 + 10log\frac{\sigma}{2f\pi\mu}\alpha\frac{\sigma}{\mu} \quad (3)$$

where, μ the relative transmittance, frequency (f), and s is is the overall conductivity. SER is the materials' permeability and conductivity function (μ), i.e. SER f (σ / μ). Thus, for the constants σ and, the SER decrease with frequency. Consequently, materials must contain carriers of mobile charges (holes or electrons) to reflect electromagnetic radiation [25].

A secondary mechanism for protection against electromagnetic interference is absorption loss (SEA). The electromagnetic wave's amplitude reduces dramatically within matter as it travels through it, according to the plane wave hypothesis [26]. So, the absorption loss is caused by heating of the material and ohmic losses owing to generated currents. The absorption loss (SEA) in decibels (dB) may be stated for conductive materials [27]:

$$SEA = 20loge_{a=}^{\alpha}8.7d\sqrt{f\pi\sigma\mu\alpha d\sigma\mu\alpha d} \quad (4)$$

where, a and d are the slab attenuation and thickness constants, respectively. The constant of attenuation determines how much the intensity of an electromagnetic wave decreases as it passes through a material. SEA depends on sample thickness

(d), transmittance (μ), and electrical conductivity (σ) [28]. This SER/SEA dependence on and specifies that in ferromagnetic conductive metals, the domination of shielding is by adsorption rather than interaction. Furthermore [29]:

$$\alpha = \frac{4\pi n}{\lambda 0} \quad (5)$$

where, n is the index of refractive and λ_0 is the wavelength in a vacuum, which in the case of non-magnetic materials is given μ-1. So,

$$\alpha = \frac{4\pi\varepsilon_2^1}{\lambda 0} \quad (6)$$

2. EXPERIMENTAL PART

In this study, a novel nano co-polymer was prepared and used in absorbing materials for electromagnetic radiation for radar, which includes:

2.1 Preparation of the polymeric nano material

The novel nano co-polymer was prepared in ratio (5: 2) as follows: In 250 mL round bottom flask, (740.5 gm, 5.0 mole) of Phthalic anhydride was dissolved in 70 ml DMSO at 110°C when the mixture became a clear solution, (184 gm, 2.0 mole) of Glycerol was then added. Along 15 min, 15 ml of p-Xylene was dropped in batches to eliminate the water molecules which are formed during the esterification reaction, then added cooled deionized water to get the suspension solution. Finally, the solid white precipitated was collected by filtration. These nanoparticles' co-polymer was characterized using a spectrum of FT-IR, H-NMR, AFM and TEM techniques.

2.2 Preparation of different mixtures proportions

Table 1 showed the mixing ratios and weights of the polymeric material and thermal dye. The mixtures were prepared based on what is mentioned in the table and on the mixing ratios and weights of the polymeric material and thermal dye that were used based on (20) g.

Table 1. Mixing ratios and weights of the polymeric material and thermal dye

Mixture No.	Nano Polymer Weight Mixing %	Nano Fe$_3$O$_4$ Weight Mixing %	Nano Polymer Weight (gr.)	Nano Fe$_3$O$_4$ Weight (gr.)	Paint Weight (gr.)	Total Mixture Weight Paint + Nano polymer +Nano Fe$_3$O$_4$ (gr.)
Paint only	---	----	---	----	----	20
1	1%	2.5%	0.2	0.5	19.3	20
2	3%	2.5%	0.6	0.5	18.9	20

2.3 Specimens

Steel pieces with dimensions of (10.5 x 10.5) cm were prepared [30-34]. After that, the surface was polished and smoothed with polishing papers (grade 400) to prepare the surface to receive the mixture, as well as to clean the surface from any sediments, oxides, dust or dirt, just like preparing the surface for car painters [35-39]. The surface was washed with

fresh water, dried for 1 hour, then cleaned with acetone or alcohol, according to what is customary among scientific sources. After the cleaning process, a base layer primer was used to increase the adhesion, as a primer from (model thick primer filler, WURTH, Germany) [40, 41]. The paint (heat resistance paint, model dr ferro, black color, turkey origin) was sprayed with the addition of thinner (Nitro Cellulose thinner, Jordan origin) having a mixing ratio of 1:1, after the process

of mixing the nanomaterial, iron oxide with the thinner to be ready for paint. Figure 2 illustrates the raw materials utilized. Figure 3 illustrates the steel samples after applying the primer coat as shown in Figure 3 (a), and after applying the full mixture coat as shown in Figure 3 (b). the mixture was sprayed using an air compressor gun at 6 Bar of pressure.

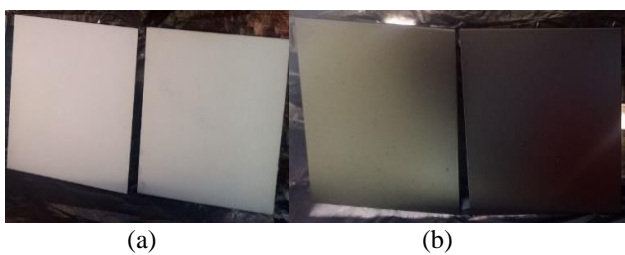

Figure 2. Raw materials used

(a)	(b)

Figure 3. Samples of the steel (a) only a primer coating paint; (b) after applying the mixture paint

A network vector analyzer (VNA) model (VectorStar, Anritsu company, Japan) was utilized to study the reflectivity loss characteristics of the samples as shown in Figure 4.

Figure 4. VNA setup

3. RESULTS AND DISCUSSION

3.1 Characterization of prepared novel nano co-polymer

Figure 5 illustrates the FT-IR diagram, which shows weak broadband at (3055 cm^{-1}) due to the alcoholic (O-H) bond and the hydrogen bond, as it showed a riding band at (3057 cm^{-1}) caused by the aromatic (C-H) bond and the riding bundles at (2871-2992 cm^{-1}) belong to the asymmetric and symmetric (C-H) bond, and a strong riding bundle at (1770-cm^{-1}) appears back to the Isterian (C=O) band, and riding bundles at (1584-1495 cm^{-1}). It refers to the (C=C) aromatic, strong sharp crest at (1069 cm^{-1}) of the esteric (C-O) bond, and the firmness appears at (734 and 897 cm^{-1}) due to the bilateral compensation on the aromatic ring. Figure 6 shows the [1]H-

NMR spectrum, which explains the single signal at 13.12ppm of the characteristic proton in the group of carboxylic acid. However, the multiplier in the region 7.48-7.79 ppm is attributed to all protons in the aromatic ring, the signals at 4.26-4.28 ppm methylene protons in the copolymer structure, and the multiply at 3.68-3.66 ppm of methyl protons, but the aliphatic alcohols signal disappeared indicating that copolymer composition.

Figures 7 (a, b) show the copolymer nanoparticles' outer surface. The copolymer surface roughness modulus was 22 nm and the sqrt was equal to (26.6) nm. This suggests that the nanoparticles dark side plays a significant importance in the surface finish, surface homogeneity and regular crystal system. Also, the average particle height was equal to 106.37 nm. Figure 8 illustrates the particle size distribution of the nano co-polymer.
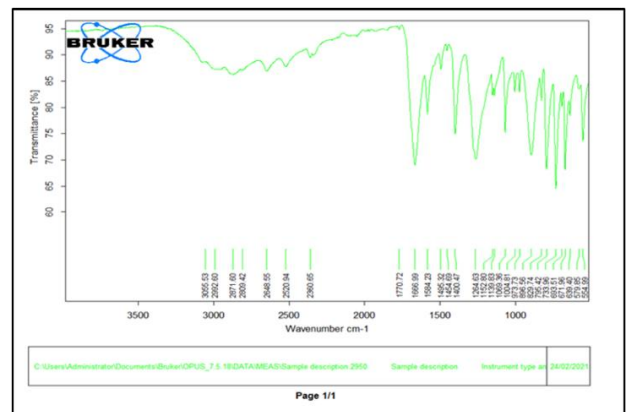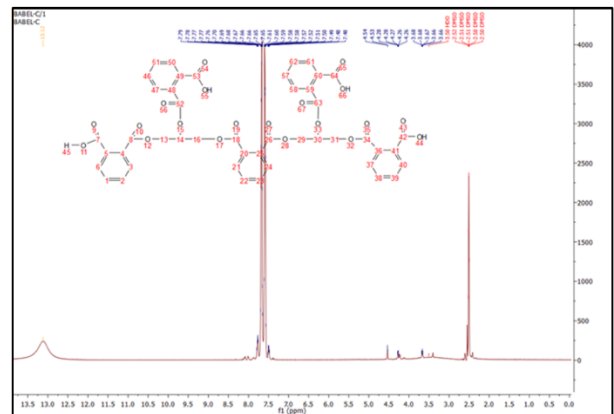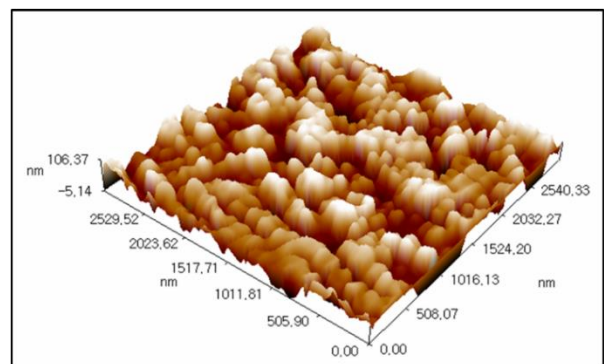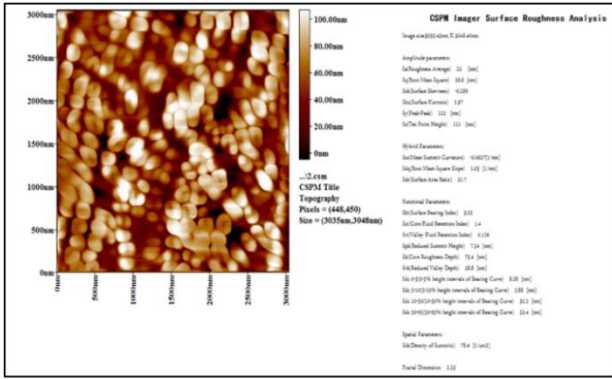

Figure 5. Nano co-polymer FT-IR

Figure 6. ^{1}HNMR Spectrum

(a)

(b)

Figure 7. (a) 3D nano co-polymer AFM Image. (b) 2D nano co-polymer AFM Image
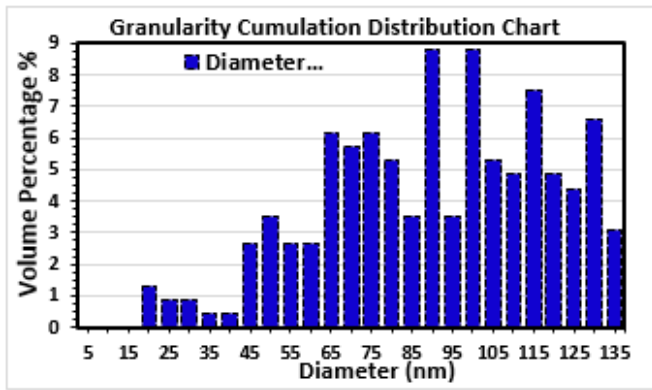

Figure 8. Nano co-polymer particle size distribution

Figure 9 illustrates the nano co-polymer TEM micrographs of nanoparticles containing irregular layer-shaped particles of different sizes and shapes on a semi-spherical shape. It was found that the average size of nanoparticles of the co-polymer is 106.37 nm.
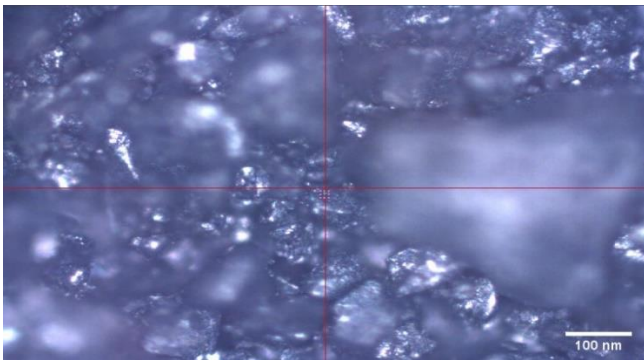

Figure 9. TEM micrographs for the nanoparticles co-polymer

3.2 Reflectivity loss

The reflectivity loss was measured with frequency for the samples that were prepared using the radar wave attenuation device and within the (x-band) 12-8 band. Figures 10 show the relationship between the loss of reflectivity and frequency without coating. When the percentage of nano polymer added

is 1%, that is, 0.2 gm to the coating, as in Figures 11 in the presence of 2.5 nanoparticles of iron oxide, it reaches 25.3 dB - at frequency 9.15 GH with other values for the reflection energy loss at different frequencies. When the percentage of nano polymers is increased to 3%, i.e. 0.4, to the thermal coating with the presence of 2.5% of iron oxide, we find that the value of the reflectivity loss increases significantly. Figures 12 show the reflectivity up to 27.2 dB at a frequency of 8.3 GH and bandwidth of (8.1-8.2 GH), thus, there is a clear attenuation of the radar waves, and we note another reflectivity value of 10.7 dB at the frequency 9.14GH, which is confined within a bandwidth of GH (9-9.3 GH). Through these results, it was found that the nanocomposite material has high properties in absorbing microwave waves and thus helped in the continuous dispersal of radiation and work to weaken it and thus absorb and attenuate the waves coming from the radar [42, 43].
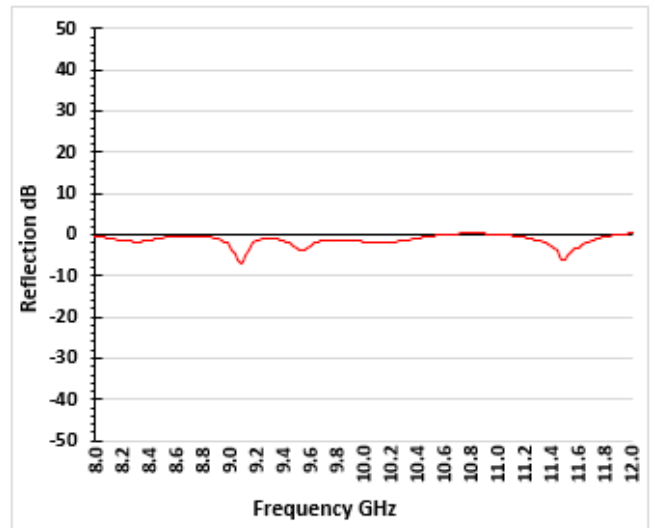

Figure 10. The relationship between reflectivity and frequency without coating metal parts
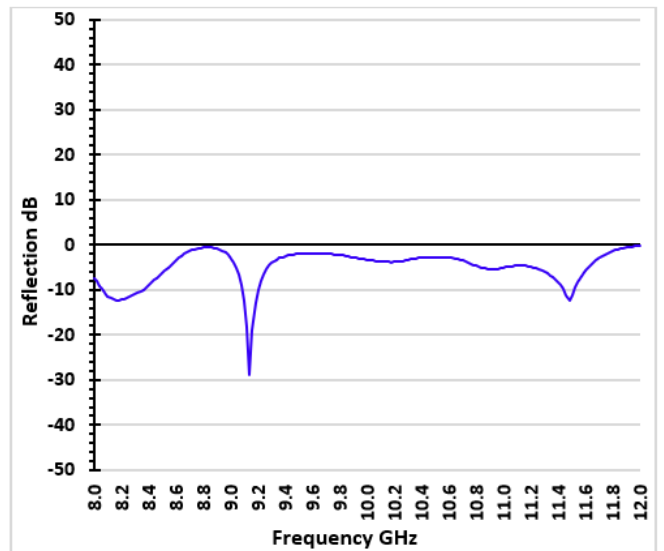

Figure 11. The relationship between reflectivity and frequency in the presence of paint (1%) nano polymer
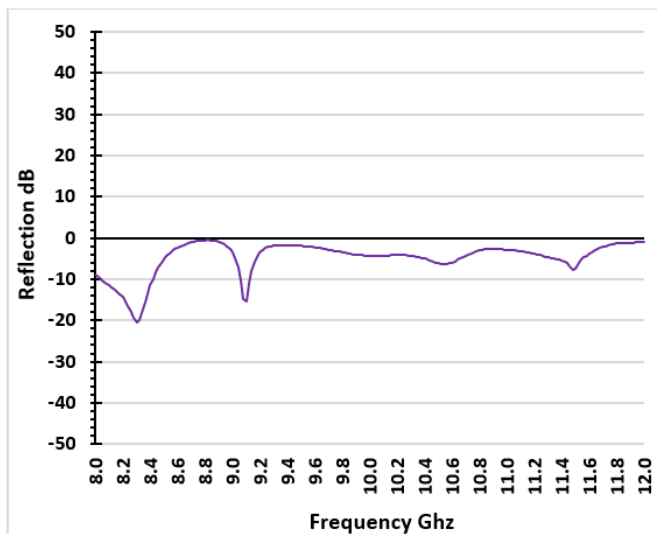
Figure 12. Shows the relationship between reflectivity and frequency in the presence of paint (3%) nano polymer

4. CONCLUSIONS

The nanoparticles copolymer was successfully synthesized using the melting process by condensation polymerization from the reaction of glycerol with phthalic anhydride with the release of water as a by-product. From the nano co-polymer AFM Images, it is clear that the nanoparticles dark side plays a significant importance in the surface finish quality, surface homogeneity and regular crystal system. From the TEM micrographs of copolymer nanoparticles which contain irregular layer-shaped particles of different sizes and shapes on a semi-spherical shape; It was found that the average size of nanoparticles of the copolymer is 106.37 nm. Results show that when the percentage of nano polymers is increased to 3%, with the presence of 2.5% of iron oxide, the value of the reflectivity loss significantly increases. For the reflectivity up to 27.2 dB at a frequency of 8.3 GHz and a bandwidth of (8.1-8.2 GHz), there is a clear attenuation of the radar waves, which is confined within a bandwidth of (9-9.3 GHz). As a consequence of this, the combination of glycerol and phthalic anhydride, with the appropriate proportions of each component, would be an appealing possibility for microwave-absorbing materials.

REFERENCES

[1] Panwar, R., Agarwala, V., Singh, D. (2015). A cost effective solution for development of broadband radar absorbing material using electronic waste. Ceram. Int., 41(2): 2923-2930. https://doi.org/10.1016/j.ceramint.2014.10.118

[2] Zhang, Z., Tan, J.W., Gu, W.H., Zhao, H.Q., Zheng, J., Zhang, B.S., Ji, G.B. (2020). Cellulose-chitosan framework/polyailine hybrid aerogel toward thermal insulation and microwave absorbing application. Chem. Eng. J., 395: 125190. https://doi.org/10.1016/j.cej.2020.125190

[3] Lin, X., Gong, H.Y., Zhang, Y.J., Zhang, L., Li, M., Wang, S., Adil, S. (2021). Targeted design and analysis of microwave absorbing properties in iron-doped SiCN/Si3N4 composite ceramics. Ceram. Int., 47(4): 4521-4530. https://doi.org/10.1016/j.ceramint.2020.10.014

[4] Ling, A., Tan, G.G., Man, Q.K., Lou, Y.X., Chen, S.W., Gu, X.S., Li, R.W., Pan, J., Liu, X.C. (2019). Broadband microwave absorbing materials based on MWCNTs' electromagnetic wave filtering effect. Compos. Part B Eng., 171: 214-221. https://doi.org/10.1016/j.compositesb.2019.04.034

[5] Cui, Y., Wu, F., Wang, J.Q., Wang, Y.B., Shah, T., Liu, P., Zhang, Q.Y., Zhang, B.L. (2021). Three dimensional porous MXene/CNTs microspheres: Preparation, characterization and microwave absorbing properties. Compos. Part A Appl. Sci. Manuf., 145: 106378. https://doi.org/10.1016/j.compositesa.2021.106378

[6] Qu, Z.J., Wang, Y., Wang, W., Yu, D. (2021). Hierarchical FeCoNiOx-PDA-rGO/WPU layers constructed on the polyimide fabric by screen printing with high microwave absorption performance. Appl. Surf. Sci., 562: 150190. https://doi.org/10.1016/j.apsusc.2021.150190

[7] Kwak, B.S., Jeong, G.W., Choi, W.H., Nam, Y.W. (2021). Microwave-absorbing honeycomb core structure with nickel-coated glass fabric prepared by electroless plating. Compos. Struct., 256: 113148. https://doi.org/10.1016/j.compstruct.2020.113148

[8] Liu, Y., Feng, Y.R., Gong, H.Y., Zhang, Y.J., Lin, X., Xie, B.Y., Mao, J.J. (2018). Microwave absorbing performance of polymer-derived SiCN (Ni) ceramics prepared from different nickel sources. J. Alloys Compd., 749: 620-627. https://doi.org/10.1016/j.jallcom.2018.03.346

[9] Zhang, M., Ma, C., Liu, H.M., Liu, Q.C. (2021). Controllable magnetic properties and enhanced microwave absorbing of Ba2Mg2Fe12O22@Ni0.5Zn0.5Fe2O4/multi-walled carbon nanotubes composites. J. Alloys Compd., 861: 158624. https://doi.org/10.1016/j.jallcom.2021.158624

[10] Zhuang, X.H., Tan, G.G., Ning, M.Q., Qi, C.Y., Ge, X.J., Yang, Z., Man, Q.K. (2021). Boosted microwave absorbing performance of Ce2Fe17N3-δ@SiO2 composite with broad bandwidth and low thickness. J. Alloys Compd., 883: 160835. https://doi.org/10.1016/j.jallcom.2021.160835

[11] Jiang, D.W., Murugadoss, V., Wang, Y., Lin, J., Ding, T., Wang, Z.C., Shao, Q., Wang, C., Liu, H., Lu, N., Wei, R.B., Subramania, A., Guo, Z.H. (2019). Electromagnetic interference shielding polymers and nanocomposites-a review. Polym. Rev., 59(2): 280-337. https://doi.org/10.1080/15583724.2018.1546737

[12] Soylu, H.M., Yurt Lambrecht, F., Ersöz, O.A. (2015). Gamma radiation shielding efficiency of a new lead-free composite material. J. Radioanal. Nucl. Chem., 305(2): 529-534. https://doi.org/10.1007/s10967-015-4051-3

[13] More, C.V, Alsayed, Z., Badawi, M.S., Thabet, A.A., Pawar, P.P. (2021). Polymeric composite materials for radiation shielding: A review. Environ. Chem. Lett., 19(3): 2057-2090. https://doi.org/10.1007/s10311-021-01189-9

[14] Allawi, M.K., Mejbel, M.K., Oudah, M.H. (2020). Iraqi gasoline performance at low engine speeds. IOP Conf. Ser. Mater. Sci. Eng., 881: 12065. https://doi.org/10.1088/1757-899x/881/1/012065

[15] Oudah, M.H., Mejbel, M.K., Allawi, M.K. (2021). R134a flow boiling heat transfer (FBHT) characteristics

in a refrigeration system. J. Mech. Eng. Res. Dev., 44(4): 69-83. https://jmerd.net/Paper/Vol.44,No.4(2021)/69-83.pdf.

[16] Allawi, M.K., Mejbel, M.K., Younis, Y.M., Mezher, S.J. (2020). A simulation of the effect of Iraqi diesel fuel cetane number on the performance of a compression ignition engine. Int. Rev. Mech. Eng., 14(3): 151-159. https://doi.org/10.15866/ireme.v14i3.18137

[17] Allawi, M., Mejbel, M., Oudah, M. (2021). Variable Valve Timing (VVT) modelling by lotus engine simulation software. Int. J. Automot. Mech. Eng., 17(4): 8397-8410. https://doi.org/10.15282/ijame.17.4.2020.15.0635

[18] Shukla, V. (2019). Review of electromagnetic interference shielding materials fabricated by iron ingredients. Nanoscale Adv., 1(5): 1640-1671. https://doi.org/10.1039/C9NA00108E

[19] Meng, F.B., Wang, H.G., Huang, F., Guo, Y.F., Wang, Z.Y., Hui, D., Zhou, Z.W. (2018). Graphene-based microwave absorbing composites: A review and prospective. Compos. Part B Eng., 137: 260-277. https://doi.org/10.1016/j.compositesb.2017.11.023

[20] Aziz, W.J., Abid, M.A., Kadhim, D.A., Mejbel, M.K. (2020). Synthesis of iron oxide (β-fe2o3) nanoparticles from Iraqi grapes extract and its biomedical application. IOP Conf. Ser. Mater. Sci. Eng., 881: 12099. https://doi.org/10.1088/1757-899x/881/1/012099

[21] Mezher, S.J., Dawood, M.O., Beddai, A.A., Mejbel, M.K. (2020). NiO nanostructure by RF sputtering for gas sensing applications. Mater. Technol., 35(1): 60-68. https://doi.org/10.1080/10667857.2019.1653595

[22] Mezher, S.J., Kadhim, K.J., Abdulmunem, O.M., Mejbel, M.K. (2020). Microwave properties of Mg–Zn ferrite deposited by the thermal evaporation technique. Vacuum, 173: 109114. https://doi.org/10.1016/j.vacuum.2019.109114

[23] Mezher, S.J., Dawood, M.O., Abdulmunem, O.M., Mejbel, M.K. (2020). Copper doped nickel oxide gas sensor. Vacuum, 172: 109074. https://doi.org/10.1016/j.vacuum.2019.109074

[24] Sharma, M., Singh, M.P., Srivastava, C., Madras, G., Bose, S. (2014). Poly (vinylidene fluoride)-based flexible and lightweight materials for attenuating microwave radiations. ACS Appl. Mater. Interfaces, 6(23): 21151-21160. https://doi.org/10.1021/am506042a

[25] Liu, Z.F., Bai, G., Huang, Y., Li, F.F., Ma, Y.F., Guo, T.Y., He, X.B., Lin, X., Gao, H.J., Chen, Y.S. (2007). Microwave absorption of single-walled carbon nanotubes/soluble cross-linked polyurethane composites. J. Phys. Chem. C, 111(37): 13696-13700. https://doi.org/10.1021/jp0731396

[26] Cheng, Y., Zhao, H.Q., Yang, Z.H., Lv, J., Cao, J.M., Qi, X.D., Ji, G.B., Du, Y.W. (2018). An unusual route to grow carbon shell on Fe_3O_4 microspheres with enhanced microwave absorption. J. Alloys Compd., 762: 463-472. https://doi.org/10.1016/j.jallcom.2018.05.261

[27] Ren, F.J., Yu, H.J., Wang, L., Saleem, M., Tian, Z.F., Ren, P.F. (2014). Current progress on the modification of carbon nanotubes and their application in electromagnetic wave absorption. RSC Adv., 4(28): 14419-14431. https://doi.org/10.1039/C3RA46989A

[28] Lu, M.M., Cao, W.Q., Shi, H.L., Fang, X.Y., Yang, J., Hou, Z.L., Jin, H.B., Wang, W.Z., Yuan, J., Cao, M.S. (2014). Multi-wall carbon nanotubes decorated with ZnO nanocrystals: Mild solution-process synthesis and highly efficient microwave absorption properties at elevated temperature. J. Mater. Chem. A, 2(27): 10540-10547. https://doi.org/10.1039/C4TA01715C

[29] Phang, S.W., Hino, T., Abdullah, M.H., Kuramoto, N. (2007). Applications of polyaniline doubly doped with p-toluene sulphonic acid and dichloroacetic acid as microwave absorbing and shielding materials. Mater. Chem. Phys., 104(2-3): 327-335. https://doi.org/10.1016/j.matchemphys.2007.03.031

[30] Mikhlif, H., Dawood, M., Abdulmunem, O., Mejbel, M.K. (2021). Preparation of high-performance room temperature ZnO nanostructures gas sensor. ACTA Phys. Pol. A, 140(4): 320-326. https://doi.org/10.12693/APhysPolA.140.320

[31] Baqer, A.R., Beddai, A.A., Farhan, M.M., Badday, B.A., Mejbel, M.K. (2021). Efficient coating of titanium composite electrodes with various metal oxides for electrochemical removal of ammonia. Results Eng., 9: 100199. https://doi.org/10.1016/j.rineng.2020.100199

[32] Mejbel, M.K., Abdullah, I.T., Taieh, N.K. (2022). Thin wall manufacturing improvement using novel simultaneous double-sided cutter milling technique. Int. J. Automot. Mech. Eng., 19(1): 6519-6529. https://doi.org/10.15282/ijame.19.1.2022.15.0734

[33] Muhmmed, A.A., Hussain, M.K., Khudadad, A.R., Mahdi, H.H., Mejbel, M.K. (2021). Mechanical behavior of laser engraved single lap joints adhered by polymeric material. Int. Rev. Mech. Eng., 15(12): 622-628. https://doi.org/10.15866/ireme.v15i12.21278

[34] Mejbel, M.K., Allawi, M.K., Oudah, M.H. (2019). Effects of WC, SiC, iron and glass fillers and their high percentage content on adhesive bond strength of an aluminium alloy butt joint: An experimental study. J. Mech. Eng. Res. Dev., 42(5): 224-231. https://doi.org/10.26480/jmerd.05.2019.224.231

[35] AL-Saadi, T.H.A., Abdulnabi, R.K., Ismael, M.N., Hassan, H.F., Mejbel, M.K. (2022). Glass waste based geopolymers and their characteristics. Revue des Composites et des Matériaux Avancés-Journal of Composite and Advanced Materials, 32(1): 17-23. https://doi.org/10.18280/rcma.320103

[36] Allawi, M.K., Oudah, M.H., Mejbel, M.K. (2019). Analysis of exhaust manifold of spark-ignition engine by using computational fluid dynamics (CFD). J. Mech. Eng. Res. Dev., 42(5): 211-215. https://doi.org/10.26480/jmerd.05.2019.211.215

[37] Al-Saadi, T.H.A., Mohammad, S.H., Daway, E.G., Mejbel, M.K. (2021). Synthesis of intumescent materials by alkali activation of glass waste using intercalated graphite additions. Mater. Today Proc., 42(5): 1889-1900. https://doi.org/10.1016/j.matpr.2020.12.228

[38] Beddai, A.A., Badday, B.A., Al-Yaqoobi, A.M., Mejbel, M.K., Al Hachim, Z.S., Mohammed, M.K.A. (2022). Color removal of textile wastewater using electrochemical batch recirculation tubular upflow cell. Int. J. Chem. Eng., 2022: 4713399. https://doi.org/10.1155/2022/4713399

[39] Abood Al-Saadi, T.H., Daway, E.G., Mohammad, S.H., Mejbel, M.K. (2020). Effect of graphite additions on the intumescent behaviour of alkali-activated materials based on glass waste. J. Mater. Res. Technol., 9(6): 14338-14349. https://doi.org/10.1016/j.jmrt.2020.10.035

[40] Mejbel, A.M.K.M.K., Khalaf, M.M., Kwad, A.M. (2021). Improving the machined surface of AISI H11 tool steel in milling process. J. Mech. Eng. Res. Dev., 44(4): 58-68. https://jmerd.net/Paper/Vol.44,No.4(2021)/58-68.pdf.

[41] Kadhim Jawad, L., Beddai, A.A., Ali Nasser, M., Kadhim Mejbel, M. (2022). Scrutinizing the physical and strength properties of fabricated date palm frond leaves particleboard. Mater. Today Proc., 57(2): 980-988. https://doi.org/10.1016/j.matpr.2022.03.396

[42] Humood, N., Abdullah, E.H., Abu Alais, S.M., Rashid, F.L., Hadi, A., Hashim, A. (2021). Polymer–CoFe2O4 nanocomposites as flexible microwave-radiation absorbing and high corrosion resisting CoatingMaterials for biological applications. Nanosistemi, Nanomater. Nanotehnologii, 19(3): 689-695. https://www.imp.kiev.ua/nanosys/en/articles/2021/3/nano_vol19_iss3_p0689p0695_2021_abstract.html.

[43] Hashim, A., Abdullah, E.H., Rashid, F.L., Hadi, A. (2021). Gamma- and X-Rays' shielding of new nanomaterials for biomedical applications. Nanosistemi, Nanomater. Nanotehnologii, 19(3): 697-705. https://www.imp.kiev.ua/nanosys/en/articles/2021/3/nano_vol19_iss3_p0697p0705_2021_abstract.html.